Short-Pulse Three-Dimensional Scattering From Moderately Rough Surfaces: A Comparison Between Narrow-Waisted Gaussian Beam Algorithms and FDTD

Vincenzo Galdi, *Senior Member, IEEE*, Panagiotis Kosmas, *Member, IEEE*, Carey M. Rappaport, *Fellow, IEEE*, Leopold B. Felsen, *Life Fellow, IEEE*, and David A. Castañon, *Senior Member, IEEE*

***Abstract*—In this paper, with reference to short-pulse three-dimensional scattering from moderately rough surfaces, we present a comparison between Gabor-based narrow-waisted Gaussian beam (NW-GB) and finite-difference time-domain (FDTD) algorithms. NW-GB algorithms have recently emerged as an attractive alternative to traditional (ray-optical) high-frequency/short-pulse approximate methods, whereas FDTD algorithms are well-established *full-wave* tools for electromagnetic wave propagation and scattering. After presentation of relevant background material, results are presented and discussed for realistic parameter configurations, involving *dispersive* soils and moderately rough surface profiles, of interest in pulsed ground penetrating radar applications. Results indicate a generally satisfying agreement between the two methods, which tends to improve for slightly dispersive soils. Computational aspects are also compared.**

***Index Terms*—Electromagnetic (EM) scattering by rough surfaces, finite-difference time-domain (FDTD) methods, Gaussian beams, ground penetrating radar.**

I. Introduction

FOR high-resolution noninvasive near-surface sensing and detection of buried objects, ground penetrating radar (GPR) has emerged as a reliable modality. Subsurface characterization is important for many applications, such as: buried waste analysis and remediation, ground-water survey, land mine detection, and excavation planning. Impulse GPR systems operate by transmitting a very short microwave pulse into the ground and observing the returning signal scattered by target objects. The relative electrical characteristics of the scattering objects, their distances from the radar, and their sizes can often be predicted with reasonable accuracy, and without ground contact. The degree of wave scattering is directly related to the size and electromagnetic (EM) contrast of the scatterer.

To computationally model the subsurface scattering process, it is necessary to accurately determine the EM fields refracting through the ground interface. In nature, the surface of the ground is usually rough, with random variation of surface height and separation between peaks. Since the degree of roughness is often a significant fraction of the length scale of the sensing geometry—the target size, its buried depth, the field wavelength—it is essential to incorporate this medium interface in field modeling. In addition, since the scattering of near-surface objects occurs in the nea rfield of GPR antenna systems, high-resolution methods are necessary. To compute the field generated by a realistic impulse GPR above and below a rough ground surface, only a limited number of models are available (for example, see [1]–[4] and the references therein). We consider the time domain Gabor-based narrow-waisted Gaussian beam (NW-GB) and finite-difference time-domain (FDTD) methods for addressing this difficult and important problem.

NW-GB algorithms have emerged during the last decade as an attractive alternative to traditional ray-optical high frequency (HF) methods in frequency-(FD) and time-domain (TD) applications. In the FD, the NW-GB propagators can be tracked effectively via the complex-source-point (CSP) technique, which reduces the computationally intensive *complex* ray tracing for collimated GB propagation and scattering to *quasireal* ray tracing, without the failure of strictly real ray field algorithms in caustic and other transition regions. NW-GB algorithms have been shown to furnish particularly efficient and robust predictions for wave propagation in complex configurations irradiated by extended planar aperture distributions (see [5] and the references therein for a recent review). In particular, these algorithms have recently been applied to two-dimensional (2-D) time-harmonic [6] and pulsed scattering [2] from, and

Manuscript received April 29, 2005; revised August 17, 2005. This work was supported in part by the Center for Subsurface Sensing and Imaging Systems (CenSSIS), under the Engineering Research Centers Program of the National Science Foundation through Award EEC-9986821. The work of L. B. Felsen was supported in part by Polytechnic University, Brooklyn, NY 11201.

V. Galdi is with the Waves Group, Department of Engineering, University of Sannio, I-82100 Benevento, Italy (e-mail: vgaldi@unisannio.it).

P. Kosmas was with the Department of Electrical and Computer Engineering, Northeastern University, Boston, MA 02115 USA. He is now with the Wireless Research Group at Loughborough University, Leicestershire, U.K. (e-mail: P.Kosmas@lboro.ac.uk).

C. M. Rappaport is with the Center for Subsurface Sensing and Imaging Systems, Department of Electrical and Computer Engineering, Northeastern University, Boston, MA 02115 USA (e-mail: rappapor@ece.neu.edu).

L. B. Felsen, *deceased*, was with the Department of Aerospace and Mechanical Engineering and the Department of Electrical and Computer Engineering, Boston University, Boston, MA 02215 USA, and also with Polytechnic University, Brooklyn, NY 11201 USA.

D. A. Castañon is with the Department of Electrical and Computer Engineering, Boston University, Boston, MA 02215 USA (e-mail: dac@bu.edu).

Digital Object Identifier 10.1109/TAP.2005.861568

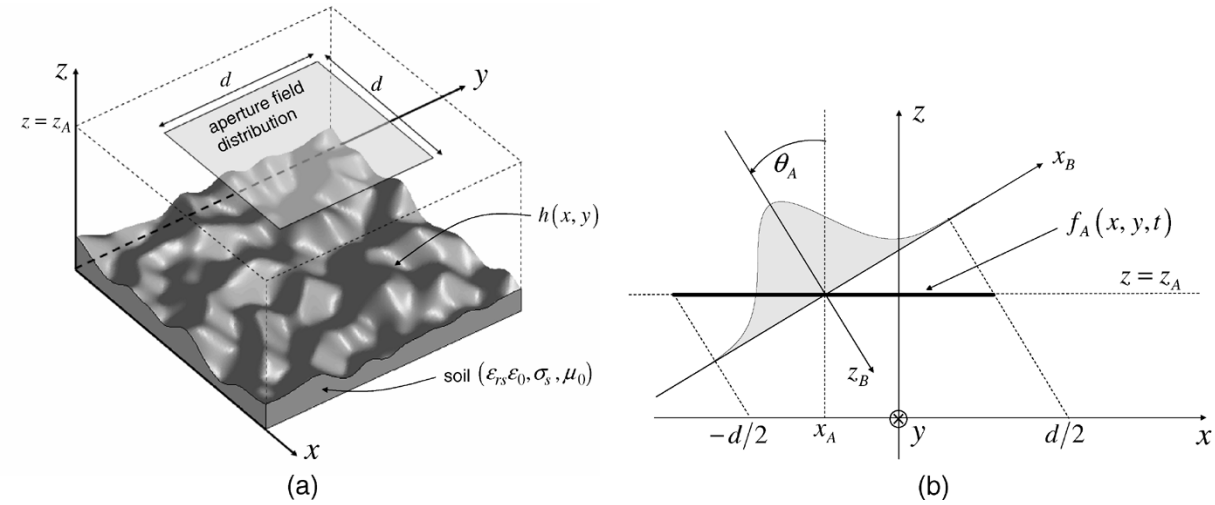

Fig. 1. Problem schematic. (a) A dielectric halfspace (soil) with relative dielectric permittivity ϵ_{rs} and electric conductivity σ_s, bounded by a moderately rough interface $z = h(x, y)$, is illuminated by an aperture-generated pulsed field impinging from free space. (b) Quasi-plane-wave tapered illumination generated by the aperture field distribution in (2) (section at $y = 0$). Parameters are chosen so that the illumination tapers to zero for $|x|, |y| > d/2$.

transmission through, moderately rough dielectric interfaces, and utilized as efficient forward solvers in *adaptive* subsurface imaging schemes [7]–[10].

For a different perspective, the reader is referred to [11]–[23], where alternative (e.g., *frame-based*, *collimated*) beam summation schemes are proposed for various propagation and scattering problems. In particular, [22] and [23] deal with wave propagation and scattering in rough-surface scenarios, using a phase-space GB summation which involves stochastic scattering matrices for the coherent and incoherent fields, and deterministic GB propagators.

In this paper, with reference to short-pulse moderately rough surface scattering, we present the three-dimensional (3-D) (vector) pulsed extension of the NW-GB algorithm; such extension will be referred to as NW pulsed-beam (NW-PB). Validation, calibration and assessment of computational utility are carried out via comparison with a solution based on a FDTD algorithm. The FDTD method [24] has been extensively studied for the problem of wave scattering from randomly rough surfaces (for example, see [3], [25] and the references therein). Although FDTD results have been previously compared to analytical solutions based on integral equation techniques [25], a direct comparison between FDTD and NW-PB results is carried out here for the first time. In addition, the FDTD algorithm used in the present work considers frequency dependent (dispersive) electric properties for the soil. Including the dispersion effect, which is most commonly omitted in previous studies, enables us to examine the applicability range of the NW-PB algorithm in relation to the electric properties of the realistic, dispersive soil.

The remainder of the paper is laid out as follows. In Section II, the problem formulation is outlined. In Section III, the NW-PB algorithm is detailed, starting with the underlying FD Kirchhoff physical optics (PO) approximation and proceding with its NW-GB parameterization and eventual analytic inversion to the TD. The FDTD implementation is described in Section IV. Numerical results and computational features are compared in Section V, for a variety of different problem parameters. Brief conclusions are given in Section VI.

II. Problem Formulation

A. Generalities

The problem geometry is illustrated in Fig. 1. A homogeneous dielectric halfspace (soil), bounded by an irregular interface described by a continuous function $h(x, y)$, is illuminated by a pulsed EM field impinging from free space [Fig. 1(a)]. In what follows, attention is restricted to the vector electric field $\mathbf{e}(\mathbf{r}, t)$, $\mathbf{r} = x\mathbf{u}_x + y\mathbf{u}_y + z\mathbf{u}_z$, from which the vector magnetic field can be computed via Maxwell's equations. Here and henceforth, bold face symbols denote vector quantities, and $\mathbf{u}$ denotes a unit vector.

B. Incident Field

The incident field $\mathbf{e}^i$ impinging on the surface with angle θ_A is assumed to be generated by a large truncated 2-D aperture of width d at height $z = z_A$, where the tangential electric field distribution $\mathbf{e}^i_{\tan}(x, y, z = z_A, t)$ is assigned

$$\mathbf{e}^i_{\tan}(x, y, z = z_A, t) = \begin{cases} f_A(x, y, t)\mathbf{u}_x, & |x - x_A|, |y| \le \frac{d}{2}, \\ 0, & \text{otherwise.} \end{cases} \tag{1}$$

In (1), x_A is a spatial shift which can be used to adjust the illumination, and, without loss of generality, an x-polarization is assumed. As in [2], attention is focused on pulsed well-collimated illuminations generated by separable linear-delay space-time field distributions

$$f_A(x, y, t) = g_A\left[(x - x_A)\cos\theta_A, y\right]\cos\theta_A \times p\left[t - c_0^{-1}(x - x_A)\sin\theta_A\right]. \tag{2}$$

In (2), $g_A(x, y)$ is a Gaussian taper function, $c_0 = (\epsilon_0\mu_0)^{-1/2}$ is the free-space wavespeed, $p(t)$ is a short pulse of length $T \ll d/c_0$, and θ_A denotes the tilt angle of the radiated beam relative to the z axis [Fig. 1(b)]. The relevant parameter configuration (c_0T, g_A, and z_A) is chosen so as to render the illumination spatial spreading and its temporal distortion negligible at the air-soil interface. Moreover, for a given incidence angle θ_A, the aperture shift x_A is adjusted so that the illumination tapers to

zero for $|x|, |y| > d/2$, as shown in Fig. 1(b). Accordingly, as in [2], in the NW-PB algorithm the incident field is approximated in terms of a pulsed tapered quasi-plane transverse-magnetic wave

$$\mathbf{e}^i(\mathbf{r},t) \sim g_A(x_B,y)p\left(t - c_0^{-1}z_B\right)\mathbf{u}_e \tag{3}$$

where $\mathbf{u}_e = (\cos\theta_A\mathbf{u}_x + \sin\theta_A\mathbf{u}_z)$, and (x_B, z_B) are beam centered coordinates [Fig. 1(b)]

$$\begin{bmatrix} x_B \\ z_B \end{bmatrix} = \begin{bmatrix} \cos\theta_A & \sin\theta_A \\ \sin\theta_A & -\cos\theta_A \end{bmatrix}\begin{bmatrix} x - x_A \\ z - z_A \end{bmatrix}. \tag{4}$$

C. Soil Model

The soil halfspace $[z < h(x,y)]$ is assumed to be nonmagnetic, homogeneous, and characterized by a relative dielectric permittivity ϵ_{rs} and an electric conductivity σ_s. The interface profile $h(x,y)$ is assumed to be *moderately* rough (both in height and slope), with undulations $\lesssim c_0T$. In realistic soil [26], the constitutive parameters ϵ_{rs} and σ_s depend on frequency in view of dispersion effects. In its present form, the NW-PB algorithm (see Section III-B) does not allow for dispersion effects, and thus the soil constitutive parameters are approximated in terms of constant values evaluated at the center frequency of the illuminating pulse. In the FDTD model (see Section IV), dispersion effects are fully taken into account.

III. The Narrow-Waisted Pulsed-Beam Algorithm

In the 2-D case detailed in [2], the TD formulation is based on a FD Kirchhoff PO approximation. In this connection, NW-PB syntheses for the reflected and transmitted fields are obtained via local (adiabatic) application of the algorithm in [27] for NW-PB synthesis of radiation from 1-D planar aperture field distributions. Here, the same route is followed, and reliance is made on the vector NW-PB synthesis developed in [28] for the radiation from 2-D planar aperture field distributions. In what follows, the FD-PO formulation is briefly reviewed, and its NW-PB discretization is presented. Discussion relies heavily on [28], with precise citations attached to each of the results extracted from there. Capital letters identify FD field quantities.

A. Frequency-Domain Formulation

In the FD formulation, the Fourier spectrum $\mathbf{E}^i(\mathbf{r},\omega)$ of the pulsed tapered quasi-plane-wave illumination $\mathbf{e}^i(\mathbf{r},t)$ in (3) is considered

$$\mathbf{E}^i(\mathbf{r},\omega) \sim g_A(x_B,y)P(\omega)\exp(ik_0z_B)\mathbf{u}_e \tag{5}$$

where (x_B, z_B) are the incident-beam coordinates in (4), $k_0 = \omega/c_0 = 2\pi/\lambda_0$ is the free-space wavenumber (with λ_0 denoting the free-space wavelength), and $P(\omega)$ is the spectrum of the pulse $p(t)$

$$P(\omega) = \int_{-\infty}^{\infty} p(t)\exp(i\omega t)dt. \tag{6}$$

The soil is described in terms of an effective complex relative permittivity

$$\epsilon_{rs}^e = \epsilon_{rs} + i\frac{\sigma_s}{\omega\epsilon_0}. \tag{7}$$

In the remainder of this section, the explicit ω-dependence in field quantities will be omitted for simplicity of notation.

1) Physical Optics Formulation: As in [2], the FD formulation here is based on the Kirchhoff physical optics (PO) approximation [29] to synthesize the reflected and transmitted fields (see also the discussion and additional references in [2, Sec. III-A]). In this framework, the FD reflected and transmitted fields ($\mathbf{E}^r$ and $\mathbf{E}^t$, respectively) are synthesized by integration of a PO equivalent magnetic surface current (EMSC) $\mathbf{J}^r_{\rm PO}$ over the illuminated interface profile (E-formulation [29])

$$\mathbf{E}^\nu(\mathbf{r}) \sim \iint_{S_{\rm PO}} \mathbf{J}^\nu_{\rm PO}(\mathbf{r}') \times \nabla G(\mathbf{r},\mathbf{r}',k^\nu)dS', \quad \nu = r \text{ or } t. \tag{8}$$

In (8), $\mathbf{r}' = x'\mathbf{u}_x + y'\mathbf{u}_y + h(x',y')\mathbf{u}_z$, $k^r = k_0$, $k^t = k_0\sqrt{\epsilon^e_{rs}}$, $S_{\rm PO}$ extends over the illuminated portion of the surface, dS' denotes the differential surface element, and G denotes the FD 3-D scalar Green's function

$$G(\mathbf{r},\mathbf{r}',k) = \frac{\exp(ikR)}{4\pi R}, \quad R = |\mathbf{r} - \mathbf{r}'|. \tag{9}$$

Following [29], the PO EMSC distributions $\mathbf{J}^r_{\rm PO}$ and $\mathbf{J}^t_{\rm PO}$ are related to the tangential reflected and transmitted fields at the air-soil interface $z = h(x,y)$ via

$$\mathbf{J}^r_{\rm PO}(\mathbf{r}') = 2\mathbf{E}^r(\mathbf{r}') \times \mathbf{u}^n, \quad \mathbf{J}^t_{\rm PO}(\mathbf{r}') = -2\mathbf{E}^t(\mathbf{r}') \times \mathbf{u}^n \tag{10}$$

with $\mathbf{u}^n$ denoting the local outward unit normal to the interface (see Fig. 2)

$$\mathbf{u}^n(\mathbf{r}') = -\frac{\nabla v(\mathbf{r}')}{|\nabla v(\mathbf{r}')|}, \quad v(\mathbf{r}') = z' - h(x',y'). \tag{11}$$

The reflected and transmitted fields at the air-soil interface are approximated by solving local canonical plane-wave scattering problems. By decomposing the incident field $\mathbf{E}^i$ into the two standard parallel ($||$) and perpendicular ($\perp$) polarization states, with respect to the local incidence plane (see Fig. 2), one obtains via straightforward plane-wave algebra [30]

$$\mathbf{E}^r = (\mathbf{E}^i \cdot \mathbf{u}^{i,||})\Gamma^{||}\mathbf{u}^{r,||} + (\mathbf{E}^i \cdot \mathbf{u}^{\perp})\Gamma^{\perp}\mathbf{u}^{\perp} \tag{12}$$

$$\mathbf{E}^t = (\mathbf{E}^i \cdot \mathbf{u}^{i,||})\tau^{||}\mathbf{u}^{t,||} + (\mathbf{E}^i \cdot \mathbf{u}^{\perp})\tau^{\perp}\mathbf{u}^{\perp} \tag{13}$$

where the dependence on the position $\mathbf{r}' = x'\mathbf{u}_x + y'\mathbf{u}_y + h(x',y')\mathbf{u}_z$ has been omitted for simplicity of notation. In (12) and (13), $\mathbf{u}^{i,||}$, $\mathbf{u}^{\perp}$, $\mathbf{u}^{r,||}$ and $\mathbf{u}^{t,||}$ are unit vectors (see Fig. 2), and $\Gamma^{||,\perp}$ and $\tau^{||,\perp}$ are Fresnel plane-wave reflection and transmission coefficients for parallel and orthogonal polarization, respectively [30]

$$\Gamma^{||} = \frac{\cos\theta^i - \sqrt{\epsilon^e_r}\cos\theta^t}{\cos\theta^i + \sqrt{\epsilon^e_r}\cos\theta^t}, \quad \tau^{||} = 1 + \Gamma^{||} \tag{14}$$

$$\Gamma^{\perp} = \frac{\cos\theta^t - \sqrt{\epsilon^e_r}\cos\theta^i}{\cos\theta^t + \sqrt{\epsilon^e_r}\cos\theta^i}, \quad \tau^{\perp} = \left(\frac{\cos\theta^i}{\cos\theta^t}\right)(1 + \Gamma^{\perp}). \tag{15}$$

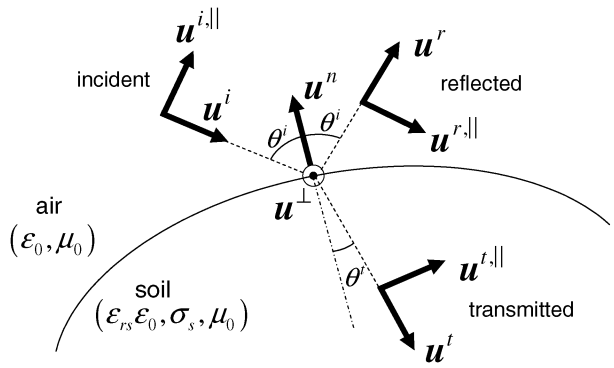

Fig. 2. Local canonical plane-wave problem schematic. Section through the local incidence plane defined by the incident field wavevector direction $\mathbf{u}_i = \sin\theta_A \mathbf{u}_x - \cos\theta_A \mathbf{u}_z$ and the local outward unit vector normal to the interface $\mathbf{u}^n$ in (11). The unit vectors $\mathbf{u}^r$ and $\mathbf{u}^t$ represent the directions of the reflected and transmitted field wavevectors, respectively. The unit vectors $\mathbf{u}^{i,\|}$, $\mathbf{u}^{r,\|}$ and $\mathbf{u}^{t,\|}$ represent the directions of the parallel-polarized ($\|$) components of the incident, reflected and transmitted fields, respectively. The unit vector $\mathbf{u}^\perp$ represents the direction of the orthogonal-polarized ($\perp$) component of the incident, reflected and transmitted fields. Incidence and transmission angles (θ^i and θ^t, respectively) are related via the Snell's law, $\sin\theta^i = \sqrt{\epsilon_{rs}}\sin\theta^t$.

Incidence and transmission angles, θ^i and θ^t, respectively (see Fig. 2), are related via the Snell's law, $\sin\theta^i = \sqrt{\epsilon_{rs}}\sin\theta^t$.

2) NW-GB Discretization: The FD-PO integrals in (8) entail radiation from a locally varying time-delayed pulsed aperture field distribution along the air-soil interface profile, and therefore are similar to the Kirchhoff *planar* (x,y)-domain aperture integrals analyzed in [28]. The analysis in [28] relies on a Gabor-based, NW-GB discretization presented in [31], [32], which is tied to a discretized lattice in a four-dimensional $(x,y;k_x,k_y)$ space-spectrum phase space, where k_x, k_y are the spectral wavenumbers. In [28], the 2-D space-time aperture field distribution is first parameterized in the FD in terms of (x,y)-domain discretized (m,p)-indexed Gabor basis functions with narrow width $L \lesssim \lambda_0$, centered on the Gabor lattice points $(x_m = mL, y_p = pL)$, with Gabor expansion coefficients approximated by aperture profile sampling at the lattice points. These initial conditions generate NW *quasiray* GB propagators, which are efficiently approximated via HF complex-source-point (CSP) asymptotics [28]. For planar apertures, *frame theory* can provide a rigorous framework to justify the validity of the underlying approximations, thereby assessing the range of applicability of the NW-GB discretization scheme (see, e.g., [14], [16], [19]).

Our formulation here is based on the local (adiabatic) application of the FD NW-GB discretization in [28, Sec. III-B]. Although nonrigorous, a similar heuristic adaptation of the NW-GB discretization scheme was applied successfully in the 2-D case [2], where, via full-wave calibration, it was found to provide satisfactory accuracy for moderate roughness and nearly-vertical incidence (see also the discussion in Section V-C). Approximating the air-soil interface at each Gabor lattice point $\mathbf{r}'_{mp} = mL\mathbf{u}_x + pL\mathbf{u}_y + h(mL,pL)\mathbf{u}_z$ as the local tangent plane, one obtains the following FD NW-GB syntheses for the reflected and transmitted field (cf. [28, Eqs. (24)–(30)])

$$\mathbf{E}^\nu(\mathbf{r}) \sim \frac{1}{2}\sum_{m,p} \mathbf{C}^\nu_{mp} \times \tilde{\mathbf{B}}^\nu_{mp}(\mathbf{r}), \quad \nu = r \text{ or } t \tag{16}$$

where

$$\mathbf{C}^\nu_{mp} \approx \begin{cases} \left(\frac{L}{\sqrt{2}}\right)\mathbf{J}^\nu_{\mathrm{PO}}\left(\mathbf{r}'_{mp}\right), & |m|,|p| \le \frac{d}{2L} \\ 0, & |m|,|p| > \frac{d}{2L} \end{cases} \tag{17}$$

$$\tilde{\mathbf{B}}^\nu_{mp}(\mathbf{r}) = ik^\nu L \frac{\exp\left[ik^\nu\left(\tilde{R}^\nu_{mp} + ib^\nu\right)\right]}{\sqrt{2}\pi\left(\tilde{R}^\nu_{mp}\right)^2} \times \left(\mathbf{r} - \mathbf{r}'_{mp} - ib^\nu \mathbf{u}^r_{mp}\right) \tag{18}$$

$$\tilde{R}^\nu_{mp} = \left|\mathbf{r} - \mathbf{r}'_{mp} - ib^\nu \mathbf{u}^\nu_{mp}\right| \tag{19}$$

$$b^r = \frac{(L\cos\theta^i)^2}{\lambda_0}, \quad b^t = \frac{\sqrt{\epsilon_r}(L\cos\theta^t)^2}{\lambda_0}. \tag{20}$$

The vector expansion coefficients $\mathbf{C}^\nu_{mp}$ in (17) are obtained via spatial sampling of the PO EMSC $\mathbf{J}^r_{\mathrm{PO}}$ and $\mathbf{J}^t_{\mathrm{PO}}$ in (10). The NW-GB CSP propagators $\tilde{\mathbf{B}}^\nu_{mp}$ in (18) are obtained from the 3-D FD Green's function in (9) by analytic continuation of the spatial coordinates into complex space via (19), with the complex displacement parameters b^r and b^t given in (20), and are launched from lattice points $\mathbf{r}'_{mp} = mL\mathbf{u}_x + pL\mathbf{u}_y + h(mL,pL)\mathbf{u}_z$ at the air-soil interface along the local reflection/transmission directions $\mathbf{u}^\nu_{mp}, \nu = r$ or t (see Fig. 2). In (18) and (19), the tilde $\tilde{}$ identifies dependence on analytically continued CSP coordinates as well as the field produced thereby. Due to the finite spatial extent of the illumination [$|x|,|y| < d/2$, see Fig. 1(b)], the summation in (16), with the approximate NW-GB coefficients in (17), involves a number $\sim (d/L)^2$ of aperture-filling beams.

B. Time-Domain Formulation

The NW-PB syntheses for reflected and transmitted fields are obtained via analytic TD inversion of the FD NW-GB syntheses in (16), along the guidelines in [28, Sec. IV]. To facilitate Fourier inversion, a few approximations are made. First, the soil parameters ϵ^e_{rs} and σ_s are assumed as frequency-independent. Next, the wavenumber in soil is approximated as [33]

$$k^t = k_0\sqrt{\epsilon^e_{rs}} \approx \sqrt{\epsilon_{rs}}\frac{\omega}{c_0} + i\kappa_s, \quad \kappa_s = \frac{\sigma_s}{2c_0\epsilon_0\sqrt{\epsilon_{rs}}} \tag{21}$$

which is legitimate in the presence of *slight* losses $\sigma_s/(\omega\epsilon_0\epsilon_{rs}) \ll 1$ over the effective bandwidth of the pulse $p(t)$. Moreover, the complex frequency-dependent Fresnel reflection and transmission coefficients in (14) and (15) are approximated by their (real, frequency-independent) values at $\sigma_s = 0$, denoted by $\bar{\Gamma}^{\|,\perp}, \bar{\tau}^{\|,\perp}$.

Anticipating Fourier inversion, the FD Gabor expansion coefficients $\mathbf{C}^\nu_{mp}$ in (17) can thus be approximated as

$$\mathbf{C}^\nu_{mp} \approx 2\mathbf{c}^\nu_{mp} P(\omega)\exp\left(i\omega t^i_{mp}\right), \quad \nu = r \text{ or } t \tag{22}$$

where, recalling (5), (10), (12), and (13)

$$t^i_{mp} = c_0^{-1} z_{Bmp}, \tag{23}$$

$$\mathbf{c}^r_{mp} = g_A(x_{Bmp}, pL) \times\left[\left(\mathbf{u}^e\cdot\mathbf{u}^{i,\|}_{mp}\right)\bar{\Gamma}^\|_{mp}\mathbf{u}^{r,\|}_{mp} + \left(\mathbf{u}^e\cdot\mathbf{u}^\perp_{mp}\right)\bar{\Gamma}^\perp_{mp}\mathbf{u}^\perp_{mp}\right] \tag{24}$$

$$\mathbf{c}^t_{mp} = g_A(x_{Bmp}, pL) \times\left[\left(\mathbf{u}^e\cdot\mathbf{u}^{i,\|}_{mp}\right)\bar{\tau}^\|_{mp}\mathbf{u}^{r,\|}_{mp} + \left(\mathbf{u}^e\cdot\mathbf{u}^\perp_{mp}\right)\bar{\tau}^\perp_{mp}\mathbf{u}^\perp_{mp}\right]. \tag{25}$$

In (23)–(25), the subscript "$_{mp}$" identifies quantities evaluated at lattice points $\mathbf{r}'_{mp} = mL\mathbf{u}_x + pL\mathbf{u}_y + h(mL, pL)\mathbf{u}_z$. Finally, the complex distance $\tilde{R}^\nu_{mp}$ in (19) [which is frequency-dependent via b^ν in (20)] is approximated in terms of its first-order Taylor expansion in b^ν

$$\tilde{R}^\nu_{mp} \approx R_{mp} - ib^\nu \frac{(\mathbf{r} - \mathbf{r}'_{mp}) \cdot \mathbf{u}^\nu_{mp}}{R_{mp}}, \quad R_{mp} = |\mathbf{r} - \mathbf{r}'_{mp}| \tag{26}$$

which was found to provide reasonably good results in the 2-D case [2]. One thus obtains the following approximate expression for the FD NW-GB propagators $\tilde{\mathbf{B}}^\nu_{mp}$ in (18)

$$\tilde{\mathbf{B}}^\nu_{mp}(\mathbf{r}, \omega) \approx -\Lambda^\nu_{mp} i\omega \exp\left[-\frac{\omega^2 (T^\nu_{mp})^2}{4} + i\omega \bar{t}^\nu_{mp}\right](\mathbf{r} - \mathbf{r}'_{mp}) \tag{27}$$

where the ω-dependence is explicitly indicated, the complex displacement $-ib^\nu \mathbf{u}^r_{mp}$ in the vector amplitude has been neglected, and

$$\Lambda^r_{mp} = -\frac{L}{\sqrt{2}\pi c_0 R^2_{mp}}, \quad t^r_{mp} = c_0^{-1} R_{mp} \tag{28}$$

$$T^r_{mp} = \frac{\sqrt{2} L \cos\theta^i}{c_0 \sqrt{\pi}} \sqrt{1 - \frac{(\mathbf{r} - \mathbf{r}'_{mp}) \cdot \mathbf{u}^r_{mp}}{R_{mp}}} \tag{29}$$

$$\Lambda^t_{mp} = -\frac{L\sqrt{\epsilon_r} \exp(-\kappa_s R_{mp})}{c_0 \sqrt{2}\pi R^2_{mp}}, \quad t^t_{mp} = c_0^{-1}\sqrt{\epsilon_r} R_{mp} \tag{30}$$

$$T^t_{mp} = \frac{\sqrt{2\epsilon_r} L \cos\theta^t}{c_0 \sqrt{\pi}} \sqrt{1 - \frac{(\mathbf{r} - \mathbf{r}'_{mp}) \cdot \mathbf{u}^t_{mp}}{R_{mp}}}. \tag{31}$$

With the above approximations, one obtains FD NW-GB syntheses for the reflected and transmitted fields that are completely analogous to the one in [28] for the radiated field. One can thus apply the analytic TD inversion procedure developed in [28, Sec. IV] for the class of Rayleigh (differentiated Gaussian) excitation pulses

$$p(t) = A_0 p^{(j)}_\varsigma \left(t - \frac{T}{2}, T\right) \tag{32}$$

$$P(\omega) = A_0 (-i\omega)^j \exp\left(i\omega \frac{T}{2}\right) P_\varsigma(\omega, T) \tag{33}$$

where A_0 is a normalization constant, the superscript $^{(j)}$ indicates jth order differentiation with respect to t, and $p_\varsigma(t)$, $P_\varsigma(\omega)$ denote the standard Gaussian pulse and its spectrum, respectively

$$p_\varsigma(t, T) = \exp\left[-\left(\frac{t}{\varsigma T}\right)^2\right]$$

$$P_\varsigma(\omega, T) = \sqrt{\pi}\varsigma T \exp\left(-\frac{\varsigma^2 T^2 \omega^2}{4}\right). \tag{34}$$

Accordingly, one obtains in a straightforward fashion the following NW-PB syntheses for the reflected and transmitted fields, $\mathbf{e}^r$ and $\mathbf{e}^t$, respectively, (cf. [28, Eqs. (53)–(55)])

$$\mathbf{e}^\nu(\mathbf{r}, t) \sim \sum_{m,p} \mathbf{c}^\nu_{mp} \times \mathbf{b}^\nu_{mp}\left(\mathbf{r}, t - t^i_{mp}\right) \tag{35}$$

where the NW-PB propagators are given by

$$\mathbf{b}^\nu_{mp}(\mathbf{r}, t) = \frac{A_0 \Lambda^\nu_{mp} \varsigma T}{\mathcal{T}^\nu_{mp}} (\mathbf{r} - \mathbf{r}'_{mp}) \times p^{(j+1)}_\varsigma \left[\left(t - \frac{T}{2} - t^\nu_{mp}\right)\varsigma, \mathcal{T}_{mp}\right] \tag{36}$$

$$\mathcal{T}^\nu_{mp} = \sqrt{(T^\nu_{mp})^2 + \varsigma^2 T^2}. \tag{37}$$

IV. FDTD Implementation

As already discussed in the introduction, the FDTD method is used in the present work to provide a reference solution for the NW-PB algorithm. Details on the well-established FDTD theory can be found in [24]. In this section, we just present some important aspects of the algorithm in relation to the application of our interest, i.e., the scattering from rough surfaces for free-space/dispersive soil interfaces.

In the present work, for the FDTD algorithm implementation, we use a total field formulation [24] based on the incident field described in Section II-B. Moreover, we consider a dispersive soil model as well as a nondispersive approximation to compare the FDTD and NW-PB results. The frequency dependent electric properties of the soil are captured using a Z-transform approach, based on a single-pole conductivity model [34]

$$\sigma_s(Z) = \frac{b_0 + b_1 Z + b_2 Z^2}{1 + a_1 Z} \tag{38}$$

where $Z = \exp(-i\omega\Delta t)$, and Δt is the FDTD time step (note that in [34] negative Z-powers are used in view of the different time convention). The relative dielectric permittivity is assumed to have a constant, average value $\epsilon_{rs} = \epsilon_r^{(av)}$, and its dependence on frequency is captured by the imaginary part of (38). This simple approach is based on the observation that for certain types of media such as soil and biological tissue, the lossy dispersive wave equation is governed almost entirely by the frequency dependent conductivity. Very good fit of the model with measured data has been observed for the electric properties of dispersive soil as well as biological tissue. The method has been compared to other standard approaches in the literature [35], and has also been validated with measured data for the soil response in a GPR experiment [36]. The nondispersive approximation considers constant permittivity and conductivity for the soil, which are calculated by the dispersive models at some central frequency of the excitation signal. Finally, a dispersive media Mur-type absorbing boundary condition (ABC) [37] was used to prevent reflections from the computational lattice boundary. This ABC was chosen due to its good performance and much less computational cost than the uniaxial perfectly matched layer (UPML) ABC.

Previous work on scattering from rough surfaces has shown that the original FDTD implementation yields accurate results for incident angles up to 45° [25]. In particular, it was shown that more accurate approximations, such as the contour path FDTD (CPFDTD), do not enhance the method's performance for smaller angles, and thus the conventional FDTD implementation is sufficiently accurate for our near normal incidence application. Another important aspect of the compatible FDTD

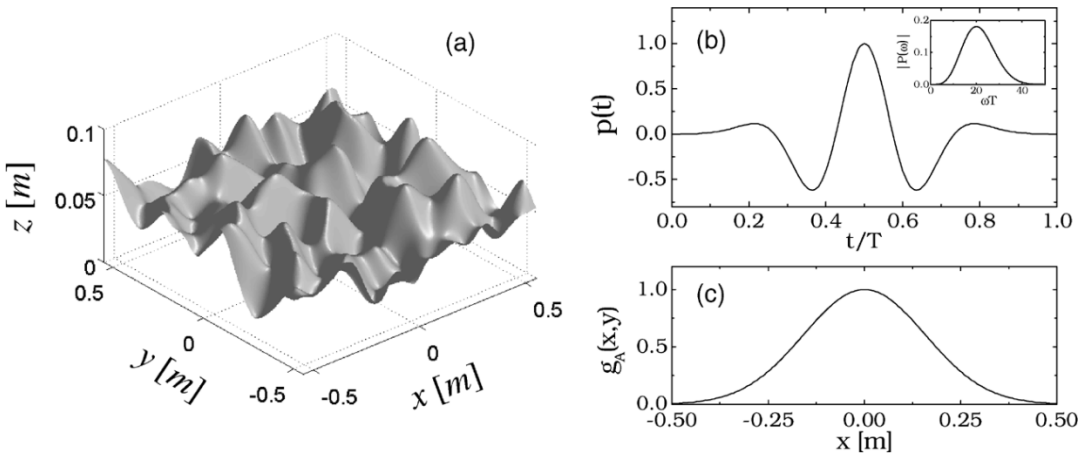

Fig. 3. Simulation geometry (cf. Fig. 1) and parameters. (a): Rough surface profile $h(x, y)$, with maximum-to-minimum height $h_{\max} \approx 0.08\,\mathrm{m}$ and maximum slope $\alpha_{\max} \approx 32°$. (b) Gaussian taper function $g_A(x, y)$ (section at $y = 0$) in (39) with $\gamma = 20\,\mathrm{m}^{-1}$ and $d = 1\,\mathrm{m}$. (c) Fourth-order Rayleigh pulse ($j = 4$, $A_0 = T^4/30\,000$, $\varsigma = 1/\sqrt{50}$) in (32) and corresponding spectrum (inset) in (33).

model is the choice of the tapered incident wave, which must ensure that diffraction artifacts are weak and do not distort the calculated results. As shown already in Section II-B, the NW-PB algorithm requires a Gaussian taper function, determined by a taper parameter γ (see Section V-A below). FDTD runs with different values of γ have confirmed that a careful choice of this parameter can minimize diffraction effects to a level that does not affect the accuracy of our results. Finally, balancing computational cost with accuracy, we choose the FDTD grid cell $\Delta = \lambda_{\min}/10$, where $\lambda_{\min}$ is the minimum significant wavelength of the excitation pulse in the soil. Therefore, the cell size Δ, and thus the FDTD time step Δt, are distinct for each pulse length and type of soil considered in the next section.

V. Numerical Results

A. Soil and Illumination Parameters

The simulation geometry considered for the parametric analysis below is illustrated in Fig. 3. Specifically, Fig. 3(a) shows the rough surface profile $h(x, y)$, which was randomly generated by extending to the 2-D case the 1-D quartic spline model in [2], [6]. Although no specific roughness model (e.g., Gaussian) was simulated, geometric parameters were selected so as to mimic natural moderate roughness with maximum-to-minimum height $h_{\max} \approx 0.08\,\mathrm{m}$ and maximum slope $\alpha_{\max} \approx 32°$. The excitation pulse $p(t)$ utilized (fourth-order Rayleigh) is shown in Fig. 3(b), and the Gaussian taper

$$g_A(x, y) = \exp\left[-\frac{\gamma^2(x^2 + y^2)}{d^2}\right] \tag{39}$$

used in the aperture field distribution in (2) is shown in Fig. 3(c). Parameters in (2) and (39) are chosen so that the illuminated region is confined in the interval $|x|, |y| < d/2$ [cf. Fig. 1(b)], with $d = 1\,\mathrm{m}$. In the parametric analysis below, a pulse length $c_0 T = 0.3\,\mathrm{m}$ (i.e., $T = 1$ ns) of potential interest in UWB GPR applications is considered. In the FDTD algorithm, this excitation is implemented as a soft source [24], with the tangential electric field assigned at grid points on the illuminating aperture, according to (1) and (2) with (39). As mentioned in the previous section, parameters are carefully selected so as to minimize truncation-induced diffraction effects.

TABLE I
Parameters for the Dispersive Soil Models at Time Steps Corresponding to Different Pulse Lengths and Soil Types

Soil type	a_1	b_0	b_1	b_2	$\epsilon_r^{(av)}$
Sand ($\Delta t = 6.0$ ps)	-0.4785	-2.183	4.023	-1.840	4.89
Sand ($\Delta t = 4.6$ ps)	-0.8785	4.867	-9.106	4.239	1.763
PR clay ($\Delta t = 4.9$ ps)	-0.8985	6.3369	-11.873	5.5378	2.0283
PR clay ($\Delta t = 3.7$ ps)	-0.9185	9.1466	-17.3662	8.2208	1.631

Moreover, two realistic soil models of interest in humanitarian demining applications are considered: a) sandy soil with 3.88% moisture, which exhibits very small dependence of its electric properties on frequency, and b) Puerto Rican (PR) clay loam which features more significant, but still moderate, loss/dispersion. The coefficients of (38) and the average relative permittivity for the two soil types and the different time steps Δt's, which depend on the pulse length $c_0 T$ and the soil constitutive parameters, are given in Table I. Dispersive soil models derived from data for the electric properties of different soil types [26] are shown in Fig. 4. As discussed in Section III-B, the present formulation of the NW-PB algorithm is based on the assumptions of *frequency-independent* soil parameters and slight losses. Accordingly, in this algorithm, the soil parameters are approximated by constant values $\epsilon_{rs}^c, \sigma_s^c$ evaluated from the dispersion curves in Fig. 4 at the center frequency of the pulse [$\omega T \approx 20$, as seen from the inset in Fig. 3(b)]. The same values are used in nondispersive FDTD simulations, for a direct comparison with the NW-PB algorithm. In addition, FDTD runs using the dispersive model are compared to the nondispersive FDTD and NW-PB approximations.

B. Results

1) Sandy Soil: We begin considering the slightly lossy/dispersive sandy soil model. From the dispersion curves in Fig. 4, the following center-frequency values are extracted for the pulse length $c_0 T = 0.3\,\mathrm{m}$ of interest: $\epsilon_{rs}^c = 4.4$, $\sigma_s^c = 0.0375\,\mathrm{S/m}$.

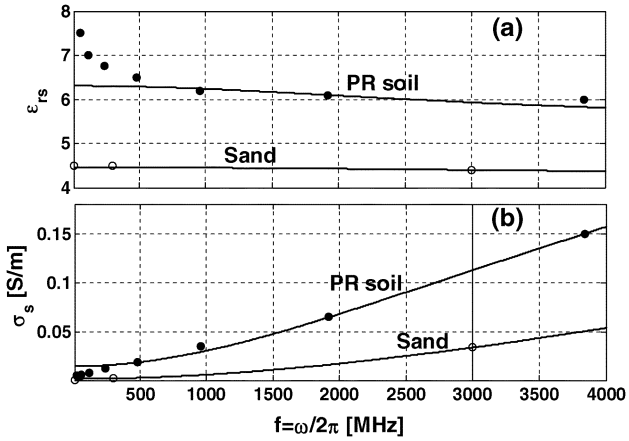

Fig. 4. Dispersion characteristics (ϵ_{rs}, σ_s versus frequency) for the two soil types considered in Section V. Dispersion is captured by the single-pole conductivity model (38), and the dots represent measured data.

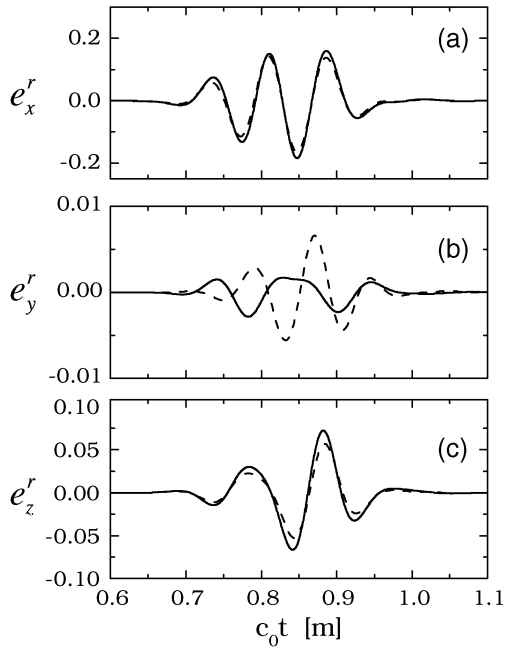

Fig. 5. Reflected field (x, y, z vector components) at observation point $x = y = 0$, $z = 0.4$ m, for sandy soil with geometry and parameters as in Figs. 1, 3, 4, and with $c_0T = 0.3$ m, $z_A = 0.35$ m, $x_A = 0$ and $\theta_A = 0$. ——— NW-PB synthesis ($\epsilon_{rs}^c = 4.4$, $\sigma_s^c = 0.0375$ S/m, and $d/L = 150$); – – – FDTD solution (full dispersive model).

Typical reflected field temporal waveforms, obtained via the NW-PB synthesis in (35) with $d/L = 150$ (i.e., 150×150 beams) are shown and compared with the FDTD solution for the three vector components in Fig. 5. Reasonably good agreement is observed for the co-polar x-component [Fig. 5(a)] and for the dominant cross-polar z-component [Fig. 5(c)]. Poorer agreement is observed for the y cross-polar component [Fig. 5(b)], which is however very weak (∼20 times smaller than the co-polar) and thus more sensitive to the various approximations involved. For the same parameter configuration, typical results for the transmitted field below the surface are shown in Fig. 6. In this case, to highlight possible soil-dispersion-induced effects, a third curve shows the FDTD solution

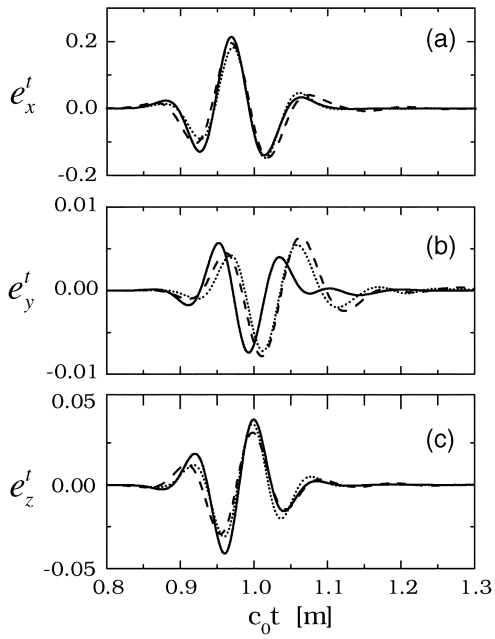

Fig. 6. As in Fig. 5, but transmitted field at subsurface observation point $x = y = 0$, $z = -0.2$ m. ——— NW-PB synthesis ($\epsilon_{rs}^c = 4.4$, $\sigma_s^c = 0.0375$ S/m, and $d/L = 150$); – – – FDTD solution (full dispersive model); · · · · · · FDTD solution (nondispersive model with $\epsilon_{rs}^c = 4.4$ and $\sigma_s^c = 0.0375$ S/m).

obtained using the same constant center-frequency soil parameters as in the NW-PB algorithm. Again, reasonably good agreement is observed. Dispersion effects are not observed to be significant for sand in this configuration, and it could be concluded that the slight disagreement between FDTD and NW-PB is most likely dominated by the other approximations involved (Kirchhoff-PO, HF asymptotics, quasi-plane-wave incidence). The same type of agreement has been observed at various observation points in the near-zone of the interface ($z = 0.4$ m and $z = -0.2$ m for reflected and transmitted field, respectively) spanning the significantly illuminated region. Satisfactory agreement has also been observed for observation points situated directly above weakly illuminated regions, as shown in Fig. 7. For a more quantitative and concise assessment of agreement and numerical convergence issues, we have computed the r.m.s. errors

$$\Delta e^{\nu}(\mathbf{r}) = \left[\frac{\int_{-\infty}^{\infty} \left| \mathbf{e}^{\nu}_{\mathrm{FDTD}}(\mathbf{r},t) - \mathbf{e}^{\nu}_{\mathrm{PB}}(\mathbf{r},t) \right|^2 dt}{\int_{-\infty}^{\infty} \left| \mathbf{e}^{\nu}_{\mathrm{FDTD}}(\mathbf{r},t) \right|^2 dt} \right]^{\frac{1}{2}} \tag{40}$$

where $\nu = r$ or t, and the subscripts "$_{\mathrm{FDTD}}$" and "$_{\mathrm{PB}}$" denote the FDTD and NW-PB solutions, respectively. For the parameter configuration in Figs. 5 and 6, the convergence of the NW-PB synthesis is illustrated in Fig. 8, where the r.m.s. errors in (40) are plotted versus the ratio d/L (∼ square root of the total number of beams). It is observed that for this configuration, values of $d/L \sim 150$ (i.e., 150×150 beams) are sufficient to stabilize the r.m.s. error around values ~ -14 dB for the reflected field and ~ -11 dB for the transmitted field. Similar values are observed moving the observation points across the significantly illuminated region, as summarized in Table II.

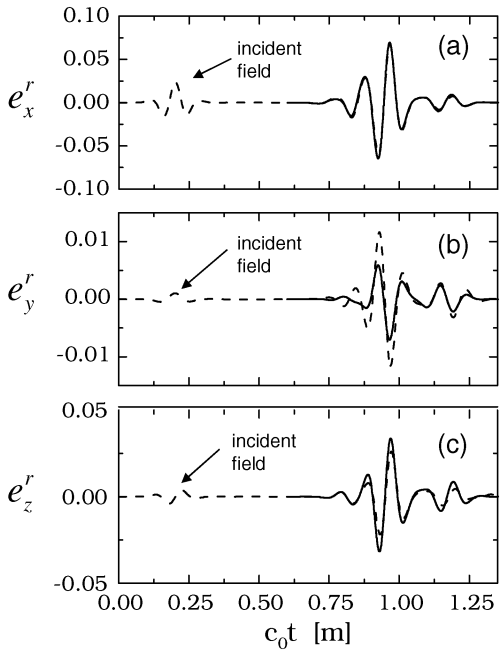

Fig. 7. As in Fig. 5, but with observation point at $x = y = -0.3$ m, $z = 0.4$ m. Incident field is also shown to highlight the weak illumination.

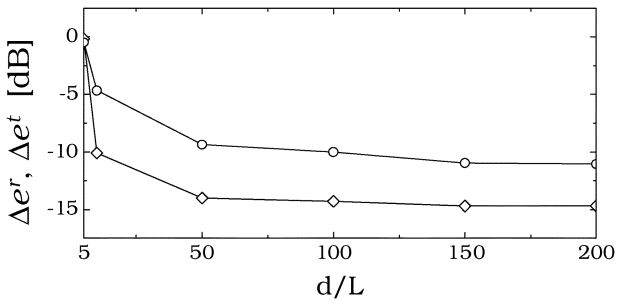

Fig. 8. As in Figs. 5 and 6, but r.m.s. errors in (40) versus the ratio d/L ($\sim$ square root of the total number of beams). The full dispersive model is considered in the FDTD solution. —◇— reflected field; —○— transmitted field.

TABLE II
PARAMETERS AS IN FIGS. 5 AND 6. R.M.S. ERRORS IN (40) FOR VARIOUS OBSERVATION POINTS SPANNING THE SIGNIFICANTLY ILLUMINATED REGION

Horizontal position	r.m.s. error [dB]	
	Reflected field ($z = 0.4m$)	Transmitted field ($z = -0.2m$)
$x = y = 0$	-14.7	-11.1
$x = y = 0.15m$	-12.8	-9.9
$x = y = -0.3m$	-15.1	-9.1
$x = 0, y = -0.15m$	-12.1	-10.5
$x = 0.3m, y = 0$	-11.2	-9.8

In order to assess its range of applicability, we strained the NW-PB algorithm by selecting parameter configurations near the limit of the range of validity of the HF Kirchhoff-PO approximation. Specifically, by conformal scaling of the profile in Fig. 1(a), we increased the roughness up to up to a maximum height $h_{\max} = 0.13$ m and a maximum slope $\alpha_{\max} = 45°$. We also considered the case of oblique incidence ($\theta_A = 30°$ and 45°). Results for three representative parameter configurations are summarized in Table III, in terms of the r.m.s. errors (40) averaged over various observations points. Deterioration of the agreement for these configurations should be attributed to the more pronounced effects of multiple reflections which are accounted for in the FDTD solution but ignored in the Kirchhoff-PO-based NW-PB synthesis. Similar results, not shown for brevity, were observed for slightly larger pulse lengths (e.g., $c_0T = 0.4$ m).

TABLE III
AS IN TABLE II, BUT FOR VARIOUS INCIDENCE ANGLES θ_A AND MAXIMUM SLOPE $\alpha_{\max}$ OF THE SOIL PROFILE. ERRORS ARE AVERAGED OVER THE FIVE REPRESENTATIVE OBSERVATION POINTS IN TABLE I. THE APERTURE OFFSET PARAMETER x_A IN (1) [SEE ALSO FIG. 1(b)] IS CHOSEN AS $x_A = -z_A \tan\theta_A$

θ_A	α_{max}	Average r.m.s. error [dB]	
		Reflected field	Transmitted field
0	45^o	-10.6	-9.3
30^o	32^o	-8.7	-8.2
45^o	32^o	-5.4	-5.3

For the slightly-lossy sandy soil, there exists a calibrated range of parameters (max slope $\alpha_{\max} \lesssim 30°$, incidence angle $\theta_A \lesssim 30°$) where NW-PB syntheses and FDTD display a reasonably good agreement (r.m.s. errors $\lesssim -10$ dB), well within the typical uncertainty arising from imperfect knowledge of soil parameters in real-world GPR applications. It is worth pointing out that the r.m.s. error metrics in (40) provide a rather *severe* assessment of the agreement, since they penalize even slight temporal misalignments between the waveforms. We also considered another performance metric, based on the maximum normalized cross-correlation (MNCC), which is probably more meaningful from a signal processing (matched filter) viewpoint; typical values were found to be around 99% for the reflected fields, and around 96% for the transmitted fields.

2) Puerto Rican Clay Loam: As a second example of application, we consider a moderately lossy/dispersive Puerto Rican (PR) clay loam soil. In this case, the following center-frequency values are extracted from the dispersion curves in Fig. 4: $\epsilon_{rs}^c = 5.89$, $\sigma_s^c = 0.122$ S/m.

From a comprehensive database of comparisons between the NW-PB syntheses and FDTD results, representative examples are shown in Figs. 9 and 10, for the reflected and transmitted waveforms, respectively. For the reflected field (Fig. 9), the dispersion effects are still negligible, and the agreement is still comparable with that observed for the sandy soil (r.m.s. error $\Delta e^r = -10.6$ dB; MNCC $= 97\%$). For the transmitted field (Fig. 10), a poorer agreement is observed (r.m.s. error $\Delta e^t = -5$ dB; MNCC $= 91\%$); this is presumably attributable to dispersion effects, which are now clearly visible from the difference between the two FDTD solutions (including and neglecting soil dispersion, respectively). Qualitatively similar results were found for other observation points spanning the illuminated region, as well as for $c_0T = 0.4$ m. Moreover, additional deterioration, qualitatively similar to that for the sandy soil case, was observed for increased roughness and oblique incidence. These results are not shown here for brevity.

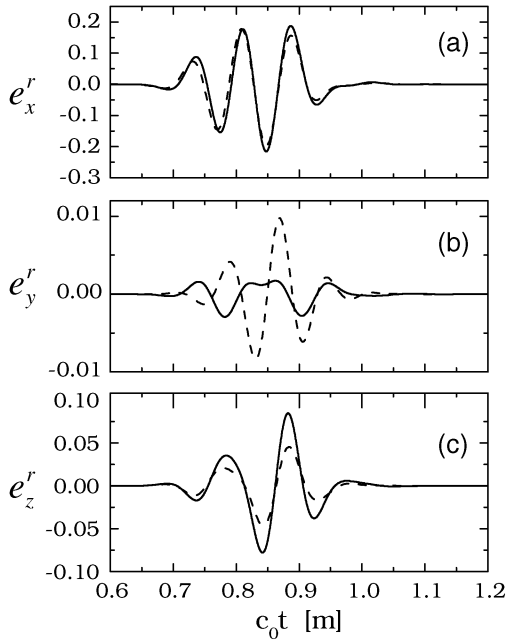

Fig. 9. As in Fig. 5, but for Puerto Rican clay loam soil ($\epsilon_{rs}^c = 5.89$, $\sigma_s^c = 0.122$ S/m). r.m.s. error $\Delta e^r = -10.6$ dB.

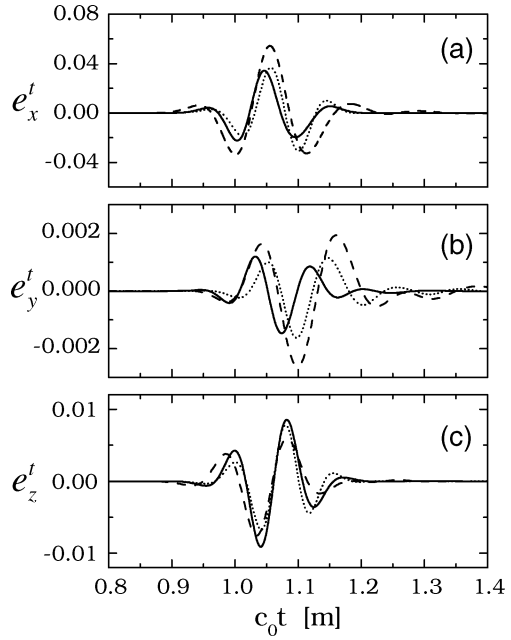

Fig. 10. As in Fig. 6, but for Puerto Rican clay loam soil ($\epsilon_{rs}^c = 5.89$, $\sigma_s^c = 0.122$ S/m). r.m.s. error $\Delta e^t = -5$ dB.

Overall, the conclusions drawn in Section V-B-1, in connection with the sandy soil model, seem to hold here for the reflected field. For the transmitted field, the less satisfying agreement is likely attributable to the nondispersive approximation in the NW-PB model.

C. Summary of Limitations in the NW-PB Algorithm

To sum up, the major limitations of the NW-PB model can be related to the various approximations involved as follows:

i) The PO-based approximation of the equivalent current, and the related local adiabatic adaptation of the NW-GB algorithm, restrict the algorithm applicability to moderate roughness ($h_{\max} \lesssim 0.5c_0T$, $\alpha_{\max} \lesssim 30°$) and nearly-vertical incidence ($\theta_A \lesssim 30°$).

ii) The NW-GB coefficient approximate estimation via PO current sampling, with beam spacings of the order of the minimum significant wavelength in the pulse, works sufficiently well in the presence of quasi-plane-wave excitation. Strong *nonlinear* delay profiles (e.g., focusing) in the illumination would require finer sampling (see, e.g., the discussion in [28]) as well as a more accurate representation of the incident field. Application of different summation schemes, as those in [11]–[23], would require nontrivial extensions in the PB propagators involved.

iii) The nondispersive approximation, which enables for analytic inversion from the FD of the NW-PB transmitted-field propagator restricts the algorithm applicability to *slightly-lossy* soils. In some real-world GPR applications, this may constitute a significant limitation.

D. Computational Features

For the NW-PB algorithm, typical running times for the examples discussed in Section V (using 150 × 150 beams) are on the order of 2 secs. per space-time vector field sample (and hence, for instance, about 8 min for the 250-point waveforms in Fig. 5) on a 1 GHz commercial laptop, with modest storage requirements (two 150 × 150 real matrices). These computing times can be reduced of almost one order of magnitude by using a coarser discretization (50 × 50 beams), at the expense of a slight accuracy deterioration (see Fig. 8). For the FDTD algorithm, the cost is orders of magnitude higher: Depending upon the excitation pulse spectrum and the soil electric properties, which will determine the choice of Δ and therefore the grid size, execution running times on 667 MHz, 16 gigabyte RAM processors can range from one to several hours, while the storage requirements range from approximately one to several gigabytes of RAM. However, for a fair comparison, it should be noted that the FDTD algorithm entails field calculation over the *entire* space-time computational domain, whose discretization is essentially dictated by accuracy and stability requirements.

VI. Conclusion

In this paper, we have presented a comparison between FDTD and NW-PB algorithms for pulsed 3-D scattering from moderately rough surfaces, which has demonstrated a satisfying agreement between the two methods. This agreement depends on several parameters of the problem, and is better for soil types that are only slightly dispersive. Despite some limitations of the NW-PB algorithm, its computational advantage over the FDTD in determining the fields at isolated points can be particularly important for its use in iterative inverse scattering schemes, which are limited by computationally expensive forward models. This investigation also sets the stage for possible use of NW-PB algorithms (within FDTD-calibrated parametric ranges) in computationally affordable Monte-Carlo-based statistical approaches for rough-surface-induced clutter characterization. Also of interest in current and future research is the incorporation in the NW-PB algorithm of more sophisticated material dispersion as well as PO scattering models.

REFERENCES

[1] T. Dogaru and L. Carin, "Multiresolution time domain analysis of scattering from a rough dielectric surface," *Radio Sci.*, vol. 35, no. 6, pp. 1279–1292, Nov.–Dec. 2000.

[2] V. Galdi, L. B. Felsen, and D. A. Castañon, "Quasiray Gaussian beam algorithm for short-pulse two-dimensional scattering by moderately rough dielectric interfaces," *IEEE Trans. Antennas Propag.*, vol. 51, no. 2, pp. 171–183, Feb. 2003.

[3] C. M. Rappaport, M. El-Shenawee, and H. Zhan, "Suppressing GPR clutter from randomly rough ground surfaces to enhance nonmetallic mine detection," *Subsurface Sensing Technol. Appls.*, vol. 4, no. 4, pp. 311–326, Oct. 2003.

[4] K. W. Lam, Q. Li, L. Tsang, and C. H. Chan, "On the analysis of statistical distributions of UWB signal scattering by random rough surfaces based on Monte Carlo simulations of Maxwell equations," *IEEE Trans. Antennas Propag.*, vol. 52, no. 12, pp. 3200–3206, Dec. 2004.

[5] L. B. Felsen and V. Galdi, "Aperture-radiated electromagnetic field synthesis in complex environments via narrow-waisted Gabor-discretized Gaussian beams," *AEÜ Int. J. Electronics Comm.*, vol. 57, no. 2, pp. 84–99, Mar. 2003.

[6] V. Galdi, L. B. Felsen, and D. A. Castañon, "Quasiray Gaussian beam algorithm for time-harmonic two-dimensional scattering by moderately rough interfaces," *IEEE Trans. Antennas Propag.*, vol. 49, no. 9, pp. 1305–1314, Sep. 2001.

[7] V. Galdi, D. A. Castañon, and L. B. Felsen, "Multifrequency reconstruction of moderately rough interfaces via quasi-ray Gaussian beams," *IEEE Trans. Geosci. Remote Sensing*, vol. 40, no. 2, pp. 453–460, Feb. 2002.

[8] V. Galdi, H. Feng, D. A. Castañon, W. C. Karl, and L. B. Felsen, "Multifrequency subsurface sensing in the presence of a moderately rough air-soil interface via quasi-ray Gaussian beams," *Radio Sci.*, vol. 37, no. 6, Nov.–Dec. 2002.

[9] V. Galdi, J. Pavlovich, D. A. Castañon, W. C. Karl, and L. B. Felsen, "Moderately rough dielectric interface reconstruction via short-pulse quasi-ray Gaussian beams," *IEEE Trans. Antennas Propag.*, vol. 51, no. 3, pp. 672–677, Mar. 2003.

[10] V. Galdi, H. Feng, D. A. Castañon, W. C. Karl, and L. B. Felsen, "Moderately rough surface underground imaging via short-pulse quasi-ray Gaussian beams," *IEEE Trans. Antennas Propag.*, vol. 51, no. 9, pp. 2304–2318, Sep. 2003.

[11] B. Rao and L. Carin, "A hybrid (parabolic equation)-(Gaussian beam) algorithm for wave propagation through large inhomogeneous regions," *IEEE Trans. Antennas Propag.*, vol. 46, no. 5, pp. 700–709, May 1998.

[12] D. Lugara and C. Letrou, "Alternative to Gabor's representation of plane aperture radiation," *Electron. Lett.*, vol. 34, no. 24, pp. 2286–2287, Nov. 1998.

[13] B. Rao and L. Carin, "Beam-tracing-based inverse scattering for general aperture antennas," *J. Opt. Soc. Amer. A*, vol. 16, no. 9, pp. 2219–2231, Sep. 1999.

[14] J. M. Arnold, "Rays, beams and diffraction a discrete phase space: Wilson bases," *Opt. Express*, vol. 10, no. 16, pp. 716–727, Aug. 2002.

[15] R. Tahri, C. Letrou, and V. F. Hanna, "A beam launching method for propagation modeling in multipath contexts," *Microwave Opt. Technol. Lett.*, vol. 35, no. 1, pp. 6–10, Oct. 2002.

[16] J. M. Arnold, "A localized beam representation of high-frequency wave fields using a Wilson basis," *Radio Sci.*, vol. 38, no. 2, Nov. 2002.

[17] D. Lugara and C. Letrou, "Printed antennas analysis by a Gabor frame-based method of moments," *IEEE Trans. Antennas Propag.*, vol. 50, no. 11, pp. 1588–1597, Nov. 2002.

[18] D. Lugara, A. Boag, and C. Letrou, "Gaussian beam tracking through a curved interface: comparison with a method of moments," *Proc. Inst. Elect. Eng. Microwaves Antennas Propag.*, vol. 150, no. 1, pp. 49–55, Feb. 2003.

[19] D. Lugara, C. Letrou, A. Shlivinski, E. Heyman, and A. Boag, "Frame-based Gaussian beam summation method: theory and applications," *Radio Sci.*, vol. 38, no. 2, Apr. 2003.

[20] A. Shlivinski, E. Heyman, A. Boag, and C. Letrou, "A phase-space beam summation formulation for ultrawide-band radiation," *IEEE Trans. Antennas Propag.*, vol. 52, no. 8, pp. 2042–2056, Aug. 2004.

[21] A. Shlivinski, E. Heyman, and A. Boag, "A phase-space beam summation formulation for ultrawide-band radiation—Part II: A multiband scheme," *IEEE Trans. Antennas Propag.*, vol. 53, no. 3, pp. 948–957, Mar. 2005.

[22] G. Gordon, E. Heyman, and R. Mazar, "A phase-space Gaussian beam summation representation of rough surface scattering," *J. Acoust. Soc. Am.*, pt. 1, vol. 117, no. 4, pp. 1911–1921, Apr. 2005.

[23] ——, "Phase-space beam summation analysis of rough surface waveguide," *J. Acoust. Soc. Amer.*, pt. 1, vol. 117, no. 4, pp. 1922–1932, Apr. 2005.

[24] A. Taflove and S. C. Hagness, *Computational Electrodynamics: The Finite-Difference Time-Domain Method*. Boston, MA: Artech House, 2000.

[25] F. D. Hastings, J. B. Schneider, and S. L. Broschat, "A Monte Carlo FDTD technique for rough surface scattering," *IEEE Trans. Antennas Propag.*, vol. 43, no. 11, pp. 1183–1191, Nov. 1995.

[26] J. E. Hipp, "Soil electromagnetic parameters as functions of frequency, soil density, and soil moisture," *Proc. IEEE*, vol. 62, pp. 98–103, Jan. 1974.

[27] V. Galdi, L. B. Felsen, and D. A. Castañon, "Narrow-waisted Gaussian beam discretization for short-pulse radiation from one-dimensional large apertures," *IEEE Trans. Antennas Propag.*, vol. 49, no. 9, pp. 1322–1332, Sep. 2001.

[28] ——, "Time-domain radiation from large two-dimensional apertures via narrow-waisted Gaussian beams," *IEEE Trans. Antennas Propag.*, vol. 51, no. 1, pp. 78–88, Jan. 2003.

[29] J. Baldauf, S. W. Lee, H. Ling, and R. Chou, "On physical optics for calculating scattering from coated bodies," *J. Electromagn. Waves Appl.*, vol. 3, no. 8, pp. 725–746, Aug. 1989.

[30] R. F. Harrington, *Time-Harmonic Electromagnetic Fields*. New York: McGraw-Hill, 1961.

[31] J. J. Maciel and L. B. Felsen, "Discretized Gabor-based beam algorithm for time-harmonic radiation from two-dimensional truncated planar aperture distributions. I. Formulation and solution," *IEEE Trans. Antennas Propag.*, vol. 50, no. 12, pp. 1751–1759, Dec. 2002.

[32] ——, "Discretized Gabor-based beam algorithm for time-harmonic radiation from two-dimensional truncated planar aperture distributions. II. Asymptotics and numerical tests," *IEEE Trans. Antennas Propag.*, vol. 50, no. 12, pp. 1760–1768, Dec. 2002.

[33] T. B. Hansen and P. M. Johansen, "Inversion scheme for ground penetrating radar that takes into account the planar air-soil interface," *IEEE Trans. Geosci. Remote Sensing*, vol. 38, no. 1, pp. 496–506, Jan. 2000.

[34] C. M. Rappaport, S. Wu, and S. C. Winton, "FDTD wave propagation in dispersive soil using a single pole conductivity model," *IEEE Trans. Magne.*, vol. 35, no. 3, pp. 1542–1545, May 1999.

[35] P. Kosmas and C. Rappaport, "Modeling with the FDTD method for microwave breast cancer detection," *IEEE Trans. Microwave Theory Tech.*, vol. 52, no. 8, pp. 1890–1897, Aug. 2004.

[36] P. Kosmas, Y. Wang, and C. Rappaport, "Three-dimensional model for GPR detection of objects buried in realistic dispersive soil," in *SPIE Proc.*, vol. 4742, Orlando, FL, Apr. 2002, pp. 330–338.

[37] P. Kosmas and C. Rappaport, "A simple absorbing boundary condition for FDTD modeling of lossy, dispersive media based on the one-way wave equation," *IEEE Trans. Antennas Propag.*, vol. 52, no. 9, pp. 2476–2479, Sep. 2004.

Vincenzo Galdi (M'98–SM'04) was born in Salerno, Italy, on July 28, 1970. He received the Laurea degree *(summa cum laude)* in electrical engineering and the Ph.D. degree in applied electromagnetics from the University of Salerno, Italy, in 1995 and 1999, respectively.

From April to December 1997, he held a visiting position with the Radio Frequency Division, European Space Research and Technology Centre (ESTEC-ESA), Noordwijk, The Netherlands. From September 1999 to August 2002, he was a Postdoctoral Research Associate with the Department of Electrical and Computer Engineering, Boston University, Boston, MA. In November 2002, he became an Associate Professor of electromagnetics with the Department of Engineering, University of Sannio, Benevento, Italy, where since February 2005, he has been Associate Chair for Undergraduate Studies in Telecommunication Engineering. He is the author or coauthor of more than 100 papers published in peer-reviewed international journals and conference proceedings. His research interests include analytical and numerical techniques for wave propagation in complex environments, electromagnetic chaos, and inverse scattering.

Dr. Galdi is a Member of Sigma Xi, the Italian Electromagnetic Society, and the Italian National Institute of Nuclear Physics. He received a 2001 International Union of Radio Science Young Scientist Award.

Panagiotis Kosmas (S'03–M'05) received the Diploma in Electrical and computer engineering from the National Technical University of Athens, Greece, in 1999, and the M.S. and Ph.D. degrees in electrical engineering from Northeastern University, Boston, MA, in 2002 and 2005, respectively.

From January 2000 until February 2005, he worked as a Research Assistant at the Department of Electrical Engineering and the Center for Subsurface Sensing and Imaging Systems, at Northeastern University. Since April 2005, he has been with the Wireless Communications Research group at Loughborough University, Leicestershire, U.K., as a Postdoctoral Research Associate. His current research interests include computational electromagnetics, and the FDTD method in particular, periodic structures, as well as inverse problems and signal processing techniques.

Carey M. Rappaport (M'80–M'87–SM'96–F'06) received the S.B. degree in mathematics and the S.B., S.M., and E.E. degrees in electrical engineering in June 1982 and the Ph.D. in electrical engineering in June 1987 from the Massachusetts Institute of Technology (MIT), Cambridge.

He has worked as a Teaching and Research Assistant at MIT from 1981 to 1987, and during the summers at COMSAT Laboratories in Clarksburg, MD, and The Aerospace Corporation in El Segundo, CA. He joined the faculty at Northeastern University in Boston, MA, in 1987. He has been Professor of Electrical and Computer Engineering since July 2000. During Fall 1995, he was a Visiting Professor of electrical engineering at the Electromagnetics Institute of the Technical University of Denmark, Lyngby, as part of the W. Fulbright International Scholar Program. He has consulted for Geo-Centers, Incorporated, PPG, Incorporated, and several municipalities on wave propagation and modeling, and microwave heating and safety. He was Principal Investigator of an ARO-sponsored Multidisciplinary University Research Initiative on Demining and co-Principal Investigator of the NSF-sponsored Center for Subsurface Sensing and Imaging Systems (CenSSIS) Engineering Research Center. He has authored over 200 technical journal and conference papers in the areas of microwave antenna design, electromagnetic wave propagation and scattering computation, and bioelectromagnetics. He has received two reflector antenna patents, two biomedical device patents, and three subsurface sensing device patents.

Prof. Rappaport is a Member of Sigma Xi and Eta Kappa Nu professional honorary societies. He was awarded the IEEE Antenna and Propagation Society's H. A. Wheeler Award for Best Applications Paper, as a student in 1986.

Leopold B. Felsen, *deceased*, (S'47–M'54–SM'55–F'62–LF'90) was born in Munich, Germany, on May 7, 1924. He received the B.E.E., M.E.E, and D.E.E. degrees from the Polytechnic Institute of Brooklyn, Brooklyn, NY, in 1948, 1950, and 1952, respectively.

He emigrated to the United States in 1939 and served in the U.S. Army from 1943 to 1946. After 1952, he remained with the Polytechnic (now Polytechnic University), becoming University Professor in 1978. From 1974 to 1978, he was Dean of Engineering. In 1994, he resigned from the full-time Polytechnic faculty and was granted the status of University Professor Emeritus. He was Professor of aerospace and mechanical engineering and Professor of electrical and computer engineering at Boston University, Boston, MA (part-time). He was the author or coauthor of more than 350 papers and of several books, including *Radiation and Scattering of Waves* (Piscataway, NJ: IEEE Press, 1994). He was an Associate Editor of several professional journals and was an Editor of the *Wave Phenomena Series* (New York: Springer-Verlag). His research interests encompassed wave propagation and diffraction in complex environments and in various disciplines, high-frequency asymptotic and short-pulse techniques, and phase-space methods with an emphasis on wave-oriented data processing and imaging.

Dr. Felsen was a Member of Sigma Xi and a Fellow of the Optical Society of America and the Acoustical Society of America. He has held named Visiting Professorships and Fellowships at universities in the United States and abroad, including the Guggenheim in 1973 and the Humboldt Foundation Senior Scientist Award in 1981. In 1974 he was an IEEE Antennas and Propagation Society (APS) Distinguished Lecturer. His "Poet's Corner" appears sporadically in the IEEE/APS Magazine. He received the IEEE/APS Best Paper Award for 1969 and was best paper coauthor for 1974 and 1981. He was a contributing author to papers selected for the R. W. P. King Award for 1984, 1986, and 2000. He received the Balthasar van der Pol Gold Medal from the International Union of Radio Science (URSI) in 1975, an Honorary Doctorate from the Technical University of Denmark in 1979, the IEEE Heinrich Hertz Gold Medal for 1991, the APS Distinguished Achievement Award for 1998, the IEEE Third Millennium Medal in 2000, an honorary Laurea degree from the University of Sannio in Benevento, Italy in 2003, the IEEE Electromagnetics Award for 2003, an honorary doctorate from the Technical University of Munich, Germany in 2004, three Distinguished Faculty Alumnus Awards from Polytechnic University, and an IEEE Centennial Medal in 1984. In 1977, he was elected to the National Academy of Engineering. He served on the APS Administrative Committee from 1963 to 1966 and was Vice Chairman and Chairman for both the US (1966–1973) and the International (1978–1984) URSI Commission B.

David A. Castañon (S'68-M'79-SM'98) received the B.S. degree in electrical engineering from Tulane University, New Orleans, LA, in 1971 and the Ph.D. degree in applied mathematics from the Massachusetts Institute of Technology (MIT), Cambridge, in 1976.

From 1976 to 1981, he was a Research Associate with the Laboratory for Information and Decision Systems at MIT. From 1982 to 1990, he was Senior and Chief Research Scientist at Alphatech, Inc., Burlington, MA. Since 1990, he has been a Professor in the Department of Electrical and Computer Engineering at Boston University, Boston, MA. His research interests include stochastic control and estimation, optimization, and image processing.

Dr. Castañon served as a member of the Board of Governors of the IEEE Control Systems Society. He is also a member of the AMS, SIAM, and INFORMS.